

63-3-5

AFCRL-TDR-63-243

404740

CATALOGED BY ASTIA

AS AD NO.

**AUTOMATIC DATA PROCESSING
OF WEATHER SATELLITE DATA**

by Walter A. Marggraf

Report GDA63-0046

31 January 1963

Contract AF 19(604)-8861

Project No. 6698, Task No. 669801

DDC
MAY 28 1963

TISIA A

Prepared For

**GEOPHYSICS RESEARCH DIRECTORATE
AIR FORCE CAMBRIDGE RESEARCH LABORATORIES
OFFICE OF AEROSPACE RESEARCH
UNITED STATES AIR FORCE
Bedford, Massachusetts**

Prepared By

**GENERAL DYNAMICS/ASTRONAUTICS
San Diego, California**

404740



NOTICES

Requests for additional copies by Agencies of the Department of Defense, their contractors, and other Government agencies should be directed to the:

**ARMED SERVICES TECHNICAL INFORMATION AGENCY
ARLINGTON HALL STATION
ARLINGTON 12, VIRGINIA**

Department of Defense contractors must be established for ASTIA services or have their 'need-to-know' certified by the cognizant military agency of their project or contract.

All other persons and organizations should apply to the:

**U. S. DEPARTMENT OF COMMERCE
OFFICE OF TECHNICAL SERVICES
WASHINGTON 25, D. C.**

FOREWORD

This summary report describes the Meteorological Satellite Data Processing Study, performed under Contract AF 19(604)-8861.

The computer processes studied include ingestion of satellite pictorial data with digitization and digital pictorial display; data location, which includes rectification, automatic mosaicing, and mapping transformations; and data analysis, such as differentiation, slicing, and contouring of the data from pictorial intensity, and cloud amount determination. Data from TIROS III, Orbit 509 frames is used to demonstrate the techniques and results of rectification, mosaicing, and cloud cover amount determination. Also included are examples of reduced and full resolution digitized TIROS TV pictures.

TABLE OF CONTENTS

<u>Section</u>		<u>Page</u>
1	INTRODUCTION	1
2	SOME STUDY RESULTS	3
3	DATA INGESTION OF TIROS SATELLITE PICTORIAL DATA	7
	3.1 Digitization of Photographic Prints	7
	3.2 Direct Digitization of TIROS Video Data	7
	3.3 Data Sampling	8
	3.4 Digital Picture Display	10
4	DATA LOCATION	15
	4.1 The Photogrammetric Problem	15
	4.2 Rectification - Mosaic	17
	4.3 Output Mapping and Gridding	22
5	DATA ANALYSIS	29
	5.1 Intensity Manipulations	29
	5.1.1 Intensity Normalization	29
	5.1.2 Pictorial Intensity Differentiation	29
	5.1.3 Intensity Contouring	30
	5.1.4 Intensity Contour Filter	36
	5.1.5 Intensity - Height Determination	36
	5.1.6 Cloud Separation by Intensity Slicing	36
	5.2 Cloud Amount Determination	36
	5.3 Spectral Correlation	38
6	INFORMATION PRESENTATION	41
7	CONCLUSION	43
8	REFERENCES	45
<u>Appendix</u>		
A	RECTIFICATION MATHEMATICS	47

LIST OF ILLUSTRATIONS

<u>Figure</u>		<u>Page</u>
1	Data Processing System Block Diagram	5
2	TIROS III, Orbit 509, Frame 4 TV Monitor Picture and Digital Displays	9
3	Gray Scales for One and Two Increment Spot Separation	12
4	Plot of Gray Scale Densities	13
5	Eight Frame Mosaic of TIROS III, Orbit 509	18
6	Digital Display at 120 x 120 Resolution of Eight Frames of TIROS III, Orbit 509	19
7	Two Frame Mosaic of TIROS III, Orbit 509	20
8	Digital Display at 240 x 240 Resolution of Two Frames of TIROS III, Orbit 509	21
9	Polar Stereographic Map	24
10	Oblique Stereographic Map	24
11	Mercator Map	25
12	Oblique Mercator Map	25
13	Oblique Cylindrical Map With Equal Area Scaling	26
14	Oblique Views of Earth and TIROS III, Orbit 509 and 510 Track	27
15	Boundary Point Neighborhood	30
16	TV Monitor Picture of TIROS I, Orbit 16, Frame 24 and Boundary Points Displayed With and Without Intensity Modulation	31
17	Determining Intensity Contour Vectors From 2 x 2 Picture Neighborhoods	32
18	Vector Types Possible in 2 x 2 Neighborhoods	33
19	Photograph and Intensity Contours of West African Coast Taken From Unmanned Mercury Spacecraft, MA4	35
20	Cloud Cover Analyses for Eight Frame Mosaic of TIROS III, Orbit 509/508	39
21	TIROS III, Orbit 509 Nephanalysis	40
A-1	The Earth System and the Camera System	47

LIST OF TABLES

<u>Table</u>		<u>Page</u>
1	Position and Attitude Data for TIROS III, Orbit 509	16
2	Vector Characteristic Search Table	34

SECTION 1 INTRODUCTION

The TIROS meteorological satellite has brought about a revolution in meteorological data collection. The vast amount of data made available everyday by the satellites to the meteorological community presents an almost overwhelming analysis problem. Not only is there a large amount of data, but the operational usefulness is strictly limited by time. To take advantage of this available data in a reasonable and useful time increment, as many of the necessary utilization steps as possible should be handled by automatic means. At the same time, rapid automatic processing should speed up the numerous meteorological research tasks being conducted by permitting rapid experimentation.

The research described in this report was sponsored by the Meteorological Satellite Branch, Geophysics Research Directorate under contract AF 19(604)-8861. The contractual intent was to investigate and to define some of the possible computer processes which could be usefully applied to meteorological satellite data.

The specific study items are as follows:

- a. Investigate methods of ingesting the pictorial data into a computer and determine the resolution requirements for automatic processing.
- b. Determine the feasibility of some simple pictorial analysis techniques such as intensity contouring.
- c. Investigate the possibility of determining cloud height structure from pictorial intensity contours.
- d. Automate the generation of mapped mosaics from rectified pictorial satellite data.
- e. Investigate the feasibility of determining the amount of cloud cover over a given area.
- f. Attempt the automatic correlation of the visual and infrared satellite data to positively identify cloud, water, and land areas.

Each of these items was studied and evaluated in their relation to one another and in their importance to an overall meteorological satellite data processing system. Section 2 summarizes the key results of the study. Four major processing steps can be defined and are treated in turn in the following sections on data integration, data location, data analysis, and data presentation.

The author expresses his appreciation to the many individuals who collaborated in this study. In particular, thanks are due to Mr. B. Mendoza for his meteorological advice

GDA63-0046
31 January 1963

and general encouragement, Mr. Richard F. Klawe for continuing discussions and insight, and Mr. Harry L. Baldwin, Jr. for the Mathematical and program development of the rectification and mapping transformations.

SECTION 2

SOME STUDY RESULTS

Figure 1 is a system block diagram of the investigated computer processes in relation to one another and a possible automatic meteorological satellite data processing system.

Initially, satellite pictures were photographically enlarged, then scanned and digitized for computer ingestion by means of an opto-mechanical scanner. However, it was recognized that an efficient system could not be based on rescanning photographic print material, but that the digitization and ingestion has to proceed on a real time basis as the data is received from the satellite at the Ground Readout Station. This requirement was actively pursued; and presently, the pictorial data contained on the video data tapes is directly digitized and recorded on digital tape for subsequent processing.

The task of generating mapped mosaics of individual satellite cloud photographs by a computer method, presupposes that the pictorial data in all pictures has been accurately located on a meteorologically useful map. Mosaicing then includes automatic pictorial rectification and mapping transformations. The process of pictorial rectification, which removes the apparent distortions due to the curvature of the earth and the slanting view of the camera, could by itself be a great help to the photointerpreter. No longer would a good portion of his time be taken up in locating the picture data and in transferring the summary information to a map. He could concentrate his efforts and time on the interpretation of the rectified images, and with automatic mosaicing, on the interpretation of the mapped orbit mosaics.

The identification of cloud areas from pictorial data poses a significant problem in the simulation of some possible automatic cloud analyses. In general, a human analyst has little difficulty in identifying cloud areas, because he can easily relate the spatial distribution of pictorial intensities to cloud texture. However, no relatively simple computer process is known which could perform as a cloud recognizer. Intensity slicing has been suggested as a possible means. Since there are land, ice and sun glint areas equally as bright as areas of true cloud, no solution based on pictorial intensity thresholds alone is expected. This is true even though intensities may have been normalized by taking into account variations due to slant angle and solar illumination distribution. To alleviate this problem, the use of both visual and infrared satellite data in a spectral correlation process is expected to give positive cloud identification.

Cloud cover per unit area was determined for a rectified-mosaic of eight frames of TIROS III, Orbit 509. The chosen output map is on an oblique cylindrical projection with equal area scaling. The cloud amounts over the mosaic map were determined and printed in tenths. The result is compared to a TIROS III nephanalysis for the same orbit.

GDA63-0046

31 January 1963

The presentation of automatically extracted meteorological information, such as reported in Section 5.2 for cloud amount distribution, will involve some form of coding or contouring. Such contours of extracted information on a suitable map could be quickly assimilated by the meteorological user.

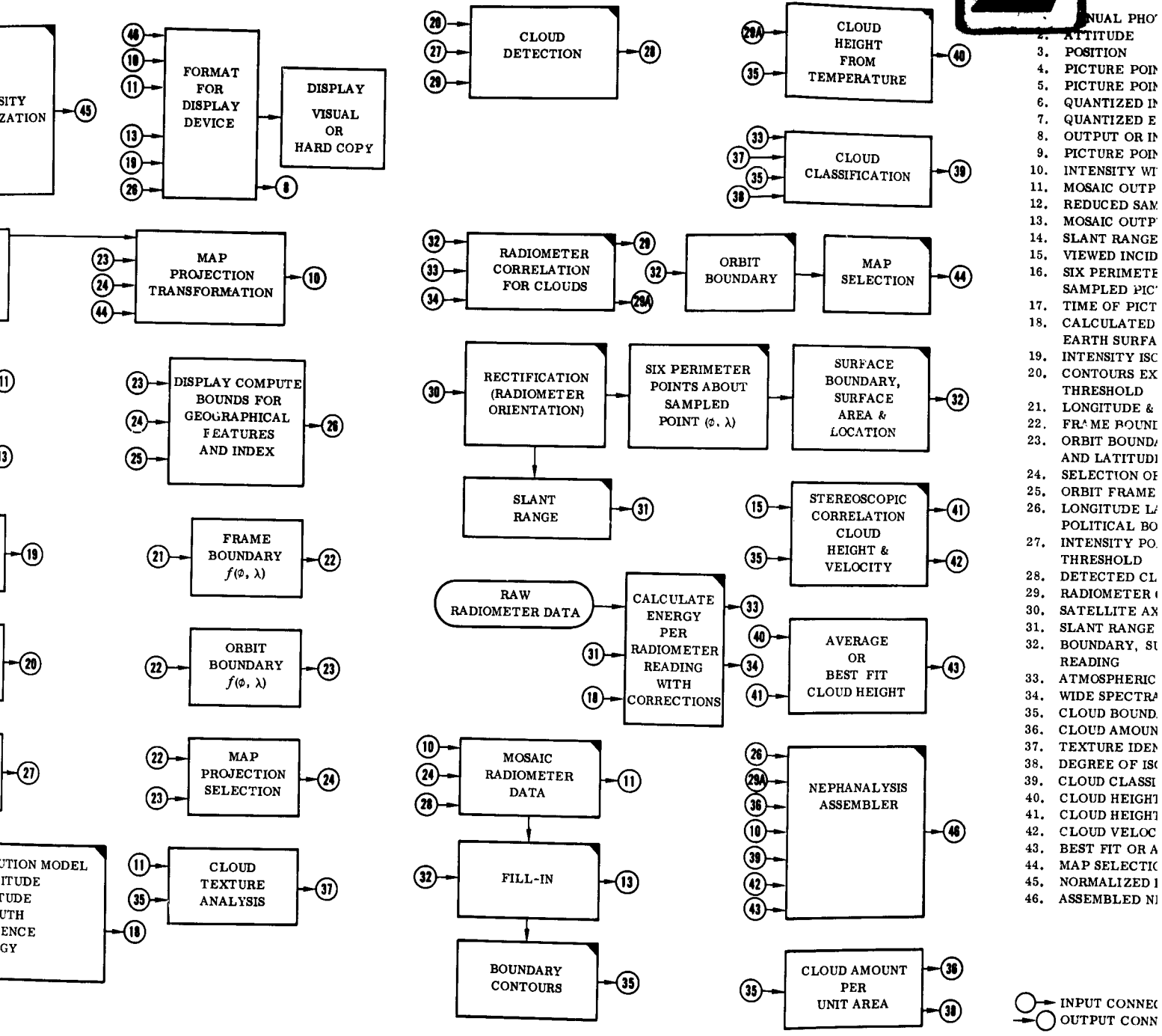
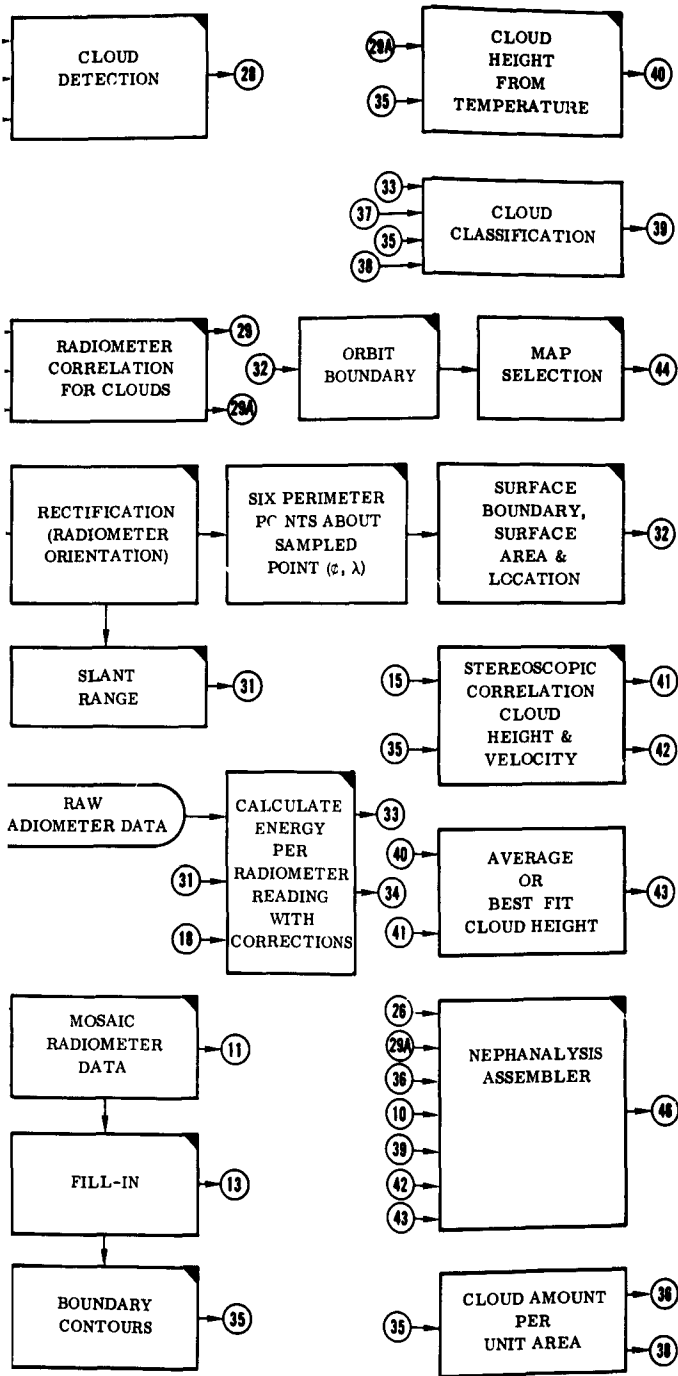


Figure 1. Data Processing



CONNECTOR IDENTIFICATION

1. MANUAL PHOTOGRAMMETRIC INTERPRETATION
2. ATTITUDE
3. POSITION
4. PICTURE POINT IDENTIFICATION
5. PICTURE POINTS IDEALIZED LOCATION IN IMAGE PLANE
6. QUANTIZED INTENSITY (UNCORRECTED)
7. QUANTIZED ENERGY (IN IMAGE PLANE)
8. OUTPUT OR INPUT TO QUICK LOOK SCHEME
9. PICTURE POINTS TRUE LOCATION IN THE IMAGE PLANE
10. INTENSITY WITH LOCATION IN MAP COORDINATES
11. MOSAIC OUTPUT WITHOUT FILL IN
12. REDUCED SAMPLE HARD COPY OUTPUT, OR FULL SAMPLE SEGMENT
13. MOSAIC OUTPUT WITH FILL IN
14. SLANT RANGE PER PICTURE POINT (TV)
15. VIEWED INCIDENCE ANGLE AND AZIMUTH PER PICTURE POINT
16. SIX PERIMETER POINTS (LONGITUDE & LATITUDE) AROUND SAMPLED PICTURE POINT FROM THE IMAGE PLANE
17. TIME OF PICTORIAL FRAME (SIDERIAL TIME BASE)
18. CALCULATED SOLAR DISTRIBUTION COINCIDENT WITH SENSOR EARTH SURFACE INTERSECTION
19. INTENSITY ISOLINE CONTOURS
20. CONTOURS EXHIBITING GRADIENTS GREATER THAN A PARTICULAR THRESHOLD
21. LONGITUDE & LATITUDE PER PICTURE POINT (TV)
22. FRAME BOUNDARY IN LONGITUDE AND LATITUDE
23. ORBIT BOUNDARY (N-OVERLAPING FRAMES) IN LONGITUDE AND LATITUDE
24. SELECTION OF TRANSFER FUNCTION FOR MAP PROJECTION
25. ORBIT FRAME DESIGNATION OR INDEX
26. LONGITUDE LATITUDE GRIDS, COASTLINES, INLAND FEATURES, POLITICAL BOUNDARIES, FOR DISPLAY
27. INTENSITY POINTS OR CONTOURS GREATER THAN A PARTICULAR THRESHOLD
28. DETECTED CLOUD POINTS OR CONTOURS
29. RADIOMETER CORRELATED CLOUD INDICATION, AND TEMPERATURE (28A)
30. SATELLITE AXIS COORDINATES REFERENCED TO EARTH
31. SLANT RANGE PER READING (RADIOMETER)
32. BOUNDARY, SURFACE AREA AND LOCATION OF RADIOMETER READING
33. ATMOSPHERIC SPECTRAL WINDOW (ENERGY)
34. WIDE SPECTRAL REGION ENERGY WINDOW
35. CLOUD BOUNDARIES
36. CLOUD AMOUNT PER UNIT AREA
37. TEXTURE IDENTIFICATION PER CLOUD
38. DEGREE OF ISOLATED CELLS PER UNIT AREA
39. CLOUD CLASSIFICATION
40. CLOUD HEIGHT INFERRED FROM TEMPERATURE
41. CLOUD HEIGHT FROM STEREOSCOPIC ANALYSIS
42. CLOUD VELOCITY FROM STEREOSCOPIC ANALYSIS
43. BEST FIT OR AVERAGE HEIGHT OF CLOUD
44. MAP SELECTION FOR RADIOMETER DATA
45. NORMALIZED INTENSITY
46. ASSEMBLED NEPHANALYSIS



LEGEND
 ○ INPUT CONNECTORS □ PROCESSING FUNCTIONS STUDIED
 → ○ OUTPUT CONNECTORS ▤ FUNCTIONS UNDER STUDY

Prepared by R. Klawa

Figure 1. Data Processing System Block Diagram

SECTION 3

DATA INGESTION OF TIROS SATELLITE PICTORIAL DATA

The computer ingestion of a picture necessitates the spatial sampling and quantizing of pictorial intensities into a discrete two-dimensional array of digital intensity values, suitable for computer storage. This section describes two methods of digitization, by means of an opto-mechanical scanner and by direct video digitization. Considerations of pictorial sampling resolution, intensity level quantization, and visual quality of computer ingested pictorial data are also discussed.

3.1 DIGITIZATION OF PHOTOGRAPHIC PRINTS. TIROS satellite pictures in the form of 10×10 photographic prints made from the TIROS film negatives were digitized by sampling the reflected light intensities as a function of position by means of a rotating drum scanner. The position of a light source and a photo multiplier tube mounted on a movable carriage was incremented once per drum revolution and determined the picture line samples. In this manner either 120 samples per line and 120 lines or 960 samples per line and 960 lines could be digitized and recorded on digital magnetic tape with an IBM 727 tape unit. The picture sampling spot size could be varied in steps of 0.01 inch from 0.01 to 0.09 inch by means of different sized apertures mounted in the focal plane of the photomultiplier lens system. These were chosen to correspond to the picture scan resolution increment during digitization. A sampling disc coupled to the drum provided the required sampling pulses during one scan line across the picture. This initiated the quantizing of the amplified photomultiplier signals linearly into as many as 64 digital intensity values.

The problems connected with this method of picture scanning are its inherent relatively slow speed, the necessity for precise picture position alignment for further processing, and the quality degradation caused by scanning of second or third generation photographic materials. The realization of these problems prompted an investigation into the potentials of direct video digitization.

3.2 DIRECT DIGITIZATION OF TIROS VIDEO DATA. TIROS Video Data is recorded on magnetic FM telemetering tape at the satellite read-out sites. An FM subcarrier of 85 kc is modulated with a 62.5 kc bandwidth video signal, which is extracted from the subcarrier for subsequent digitization by means of an FM discriminator. In addition, carrier and sync pulse detectors are used for gating and initiation of line sample cycles. The analog-digital converter quantizes the analog pictorial data into 16 intensity levels. Nine of these 4 bit digital samples are packed by a digital processor into 36 bit IBM 7090 data words, which are transmitted to the IBM 7090 computer for buffering and are recorded on high density digital magnetic tape. One television scan line is sampled every $7 \mu s$ for a total of 513 samples per line which

31 January 1963

gives a slightly greater sampling rate than is required. The available video bandwidth of 62.5 kc corresponds to a horizontal resolution of 500 samples per line.

In this manner all 32 TIROS video frames in one orbit can be digitized and recorded on digital tape in about two minutes. Digitization can be performed in one pass of as many TIROS orbits as can be recorded on one reel of FM telemetering tape.

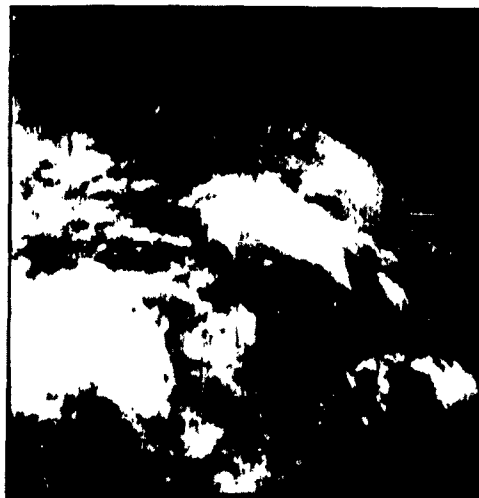
The advantages, aside from high speed and low cost, of direct video digitization are that the registration of pictures is as good as the sensor vidicon scan precision, and the degradation due to scanning of photographic materials is avoided.

3.3 DATA SAMPLING. A number of programs were written for controlled sampling experiments, for quick-look checkout, and for frame identification. These sampling programs allow the selection of different resolutions and number of gray levels from the same digital pictorial data tape. Specifically, digitized pictures on tape were sampled and displayed as 480×480 , 240×240 , and 120×120 arrays of pictorial intensity points with 16 levels of intensity. A 480×480 displayed picture consists of the first 480 intensity samples of the first 480 television scan lines. The reduced resolution pictures are obtained by displaying every other or every fourth digital intensity sample. An example follows. Figure 2a is a print of the TV monitor negative for frame 4, TIROS III, Orbit 509. The video data for TIROS III, Orbit 509 was digitized and recorded on digital magnetic tape directly from the video tape. Figures 2b, 2c, and 2d are the 480, 240 and 120 line resolution digital display pictures respectively, obtained by sampling from the digital picture tape. It appears that 240 lines maintain most of the cloud detail visible with 480 lines and that 120 lines preserve a great deal of the large scale cloud features. It should be mentioned that the FM discriminator used during the digitization of this orbit had only a 20 kc bandwidth instead of 62.5 kc, which severely limited the rate of change of intensity values in a line. This accounts for the horizontal blurring noticeable in comparing the 480 line digital picture to the TV monitor print.

Early sampling experiments with drum scanned pictures indicated that 16 levels of intensity represents about the limit of print fidelity. Consequently, the use of more intensity levels during digitization does not result in maintaining a substantially greater information content. This seems to be supported also by the TIROS video data. Observations of the analog video signal both at the TIROS read-out station and at the General Dynamics/Astronautics facility, indicate an amplitude noise level of about $1/20$ of the maximum signal amplitude. The maximum video amplitude range obtainable from the FM tape corresponds to ideal maximum black and all-white levels at subcarrier frequencies of 96 kc and 70 kc respectively. However, for typical TIROS III video frames the realized black-to-white signal ranges are considerably smaller. From frames which include the earth horizon, it was observed that space black signal levels correspond to frequencies between 96 kc to 92 kc, and that the brightest intensity levels are obtained from subcarrier frequencies close to 80 kc.



a. TV Monitor Picture



b. Digital Display at 480 x 480



c. Digital Display at 240 x 240



d. Digital Display at 120 x 120

Figure 2. TIROS III, Orbit 509, Frame 4 TV Monitor Picture and Digital Displays

This limited subcarrier range of 12 kc to 16 kc was quantized linearly into 16 intensity levels for all the TIROS III, Orbit 509 frames included in this report. This means that one digital intensity level corresponds to a frequency change of the subcarrier of between 12/15 kc to 16/15 kc. The observed video signal noise can be likened to an equivalent subcarrier change of one-twentieth of the maximum subcarrier frequency range, giving a noise frequency change of 26/20 kc. Therefore, the quantizing steps used are smaller than the observed noise amplitudes. Spreading 16 intensity levels over the maximum possible video range would result in an equivalent frequency change of 26/15 kc, which is a quantizing step greater than the equivalent noise amplitude. Digitizing over the limited range of video signals, resulted in slightly better pictorial contrast in the displayed pictures.

This investigation into video quantization raised more questions than it answered. One may ask what quantitative measure do the digital intensity values correspond to? They appear to be almost arbitrary values, bearing meaning relative only to one another, and therefore, being useful only when displayed pictorially. From the data processing standpoint, such intensity values should be calibrated to some reference, so that meaningful quantitative analyses can be performed. Who can tell whether a satellite cloud detail is bright or dark - bright or dark relative to what, when mere under or over exposure can change the relative pictorial intensity? This is analogous to under exposing sun-drenched western scenes in movie making to give the impression of a clear moonlit night! Another question, which is actually contained in the first one, is: to what extent can video intensity calibration help in rendering the video data sensing and gathering system independent of incidental changes in its environment? The TIROS video system responds adversely to sensitivity changes, such as are caused by camera warm up, vidicon phosphor sensitivity changes and by other hidden sources such as tape transport speed and local vidicon contrast variation. One intensity reference is available on the satellite in the space background, another in the sun. A field of space background and an attenuated sun field could be focused by appropriate instrumentation on the vidicon screen, thereby referencing the system to these calibration sources at all times. Some such method will become imperative, if the automatic video data processing is to have maximum meaning in the future.

3.4 DIGITAL PICTURE DISPLAY. To display and produce photographic copies of satellite pictorial data, the digitized video data is processed by a display format program and displayed on a General Dynamics/Electronics 4020. Point by point plotting of intensity values is used. Each point is exposed for a time proportional to the digital intensity value. The display format program can also be used to display the rectified mosaics.

At first, pictures were displayed with an intensity spot spacing of two position increments. This, however, resulted in a large amount of texturing due to unexposed spaces between spots and was therefore deemed undesirable. Displaying intensity spots one position increment apart resulted in a certain amount of spot overlap. This eliminated

coarse texturing and resulted in displays with better quality and contrasts. It should be noted again that sampled intensity values are displayed as one spot in the display and not as an array of points.

Figure 3 shows the computer generated test gray scales for printed negative film using one and two increment intensity spot spacing. Dupont 131 film was exposed at f/22 or f/32 depending upon spot spacing and developed in a D76 developer for seven minutes. A measured gray scale plot is shown in Figure 4, indicating that the film has a greater exposure range than required for the digital picture display. The film can be processed to obtain either a positive or a negative film strip. Positive frames are used for generating slide material and negative frames are used to make photographic prints.



Figure 3. Gray Scales for One and Two Increment Spot Separation

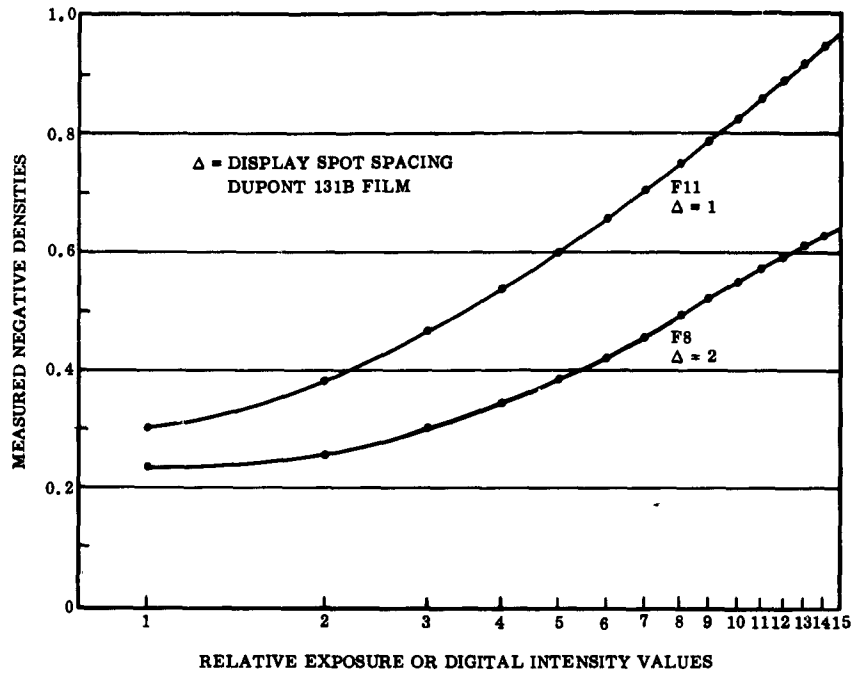


Figure 4. Plot of Gray Scale Densities

SECTION 4 DATA LOCATION

In order to mosaic several frames of satellite pictorial data by an automatic process, it is obvious that the data has to be located on the surface of the earth. The transformation of image coordinates to the corresponding earth coordinate system is the basic rectification process. The mosaicing process consists of taking individually rectified pictures and storing each in a mapping plane, whose coordinates correspond to the desired output map projection. Averaging the pictorial intensity values of overlapping picture points, and rescanning the resultant computer stored mosaic for display purposes comprise the additional tasks of the mosaic process.

This section deals with the photogrammetric problem of determining the transformation parameters, which are necessary for rectification; a description of the rectification mosaic process; and an account of the output mapping and gridding problem.

4.1 THE PHOTOGRAMMETRIC PROBLEM. In order to accomplish the rectification of each individual picture, it is necessary to have the following information:

- a. The geometry of the camera.
- b. The distortion introduced by the lens and the system electronics.
- c. The location of the satellite at the time of picture-taking.
- d. The orientation of the satellite at the time of picture-taking.

The geometry of the camera includes knowledge of the focal length of the lens and the angular coverage of the camera. This information was obtained from camera information and target photographs contained in Documentation for TIROS III Television Data (see Reference 1). Examination of the target photographs determined two functions which compensate for the distortion of each picture point location.

The location of the satellite at the time of picture-taking was obtained by combining information from picture timing data presented in TIROS III Attitude Summary (see Reference 2) and from position data given in Reference 1. The orientation of the camera was obtained by defining a coordinate system fixed with respect to the satellite and obtaining a series of rotations which will align the x-y-z coordinate system of the satellite with the X-Y-Z coordinate system of an earth-fixed, earth-centered, rotating equatorial system. These rotations are:

1. A rotation about the spin axis of the satellite (which equals the optical axis of the camera) until the principle plane (the plane formed by the optical axis and the line joining the satellite and its subpoint) is coincident with the x-y plane.

2. A rotation about the y axis until the x axis is vertical.
3. A rotation about the x axis until the x-z plane includes the Z axis.
4. A rotation about the y axis until the x-y plane is parallel to the X-Y plane.
5. A rotation about the z axis until the axes of the camera system are parallel to those of the earth system.

Each of the above rotations can be represented by a rotation matrix. Multiplication of the five matrices yields the rotation matrix corresponding to the photograph. Rotation matrices and position vectors were formed for the 32 pictures of orbit number 509. The satellite subpoint locations, the nadir angle, and azimuth angle for frames 2, 5, 8, 11, 14, 17, 20, and 23 of TIROS III, Orbit 509 are given in Table 1.

Table 1. Position and Attitude Data for TIROS III, Orbit 509

FRAME	SATELLITE SUB POINT LOCATIONS		IMAGE PLANE ORIENTATION			HEIGHT (KM)
	LONGITUDE EAST	LATITUDE NORTH	AZIMUTH	NADIR	ROLL	
2	-86.40	24.70	46.85	41.75	-5.25	811
5	-90.10	21.00	45.70	36.40	-1.60	812
8	-93.80	17.20	44.65	31.00	2.15	813
11	-97.20	13.40	44.30	25.60	6.20	814
14	-100.60	9.50	44.95	20.20	10.65	815
17	-103.80	5.60	47.00	14.80	16.00	816
20	-107.10	1.50	50.95	9.45	23.35	816
23	-110.30	-2.50	65.10	4.10	40.80	816

The angles corresponding to the above rotations can be found in the following manner. Rotation 5 is through the longitude of the subpoint of the satellite at the time of picture taking. Rotation 4 is through the latitude of the subpoint. Rotation 3 is through the azimuth of the line from the subpoint to the principle point at the time of picture taking; this azimuth is obtained as a function of three quantities: 1) the azimuth (A_0) of the satellite track at the time of picture taking, 2) the minimum nadir angle (η_0), and 3) the degrees of great circle arc (ω) over which the subpoint of the satellite has passed since the time of the minimum nadir angle. The azimuth (A), measured clockwise from north, is given by

$$A = A_0 + \cot^{-1} \left[\cot \eta_0 \sin \omega \right]$$

Rotation 2 is through the nadir angle (η), where η at picture taking time is given by

$$\cos \eta = \cos \eta_0 \cos \omega$$

Rotation 1 is through the spin angle. The spin angle at the time of minimum nadir angle is defined as the angle which would be measured on a photograph (if a photograph had been taken at this time) between a reference side of the photograph and the line perpendicular to the horizon and through the principle point. At any other time the measured angle is the sum of the spin angle and the change in azimuth since the time of minimum nadir angle. Since this change of azimuth is known, the spin angle for photographs which have a visible horizon could be measured. The rate of spin is constant, so a plot of spin angle vs time for the photographs with visible horizons is a straight line. Extrapolation yields the spin angles for all photographs.

In summary, location of the data can be in error due to vehicle position errors, attitude errors, and due to the vertical height of clouds. The following information should be retained for each picture point for some of the subsequent analyses, such as intensity normalization:

- a. Latitude and longitude of the apparent image earth point.
- b. Azimuth and nadir to the image earth point.
- c. Time (year, day, hour).

It is essential for future automatic rectification processing systems that the transformation parameters be determined in real time from tracking data and from satellite telemetered attitude data and that manual photogrammetric determinations be eliminated except for emergency situations.

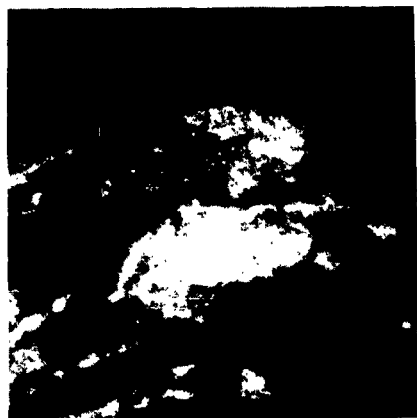
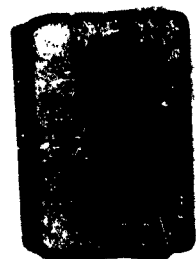
4.2 RECTIFICATION - MOSAIC. Two examples of automatic mosaicing are included. Eight frames of TIROS III, Orbit 509 were rectified and mosaiced as shown in Figure 5. The individual frames were sampled to a resolution of 120×120 picture points, with four bit intensity values. These are shown in Figure 6a through 6h. The second example is a two frame mosaic, shown in Figure 7, in which each frame was sampled with a 240×240 picture point resolution (see Figure 8). The sampled frames and their corresponding transformation matrices, which include both the rectification and mapping parameters, are made available to the rectification-mosaic program. The approximate frame outlines were transformed to the output mapping plane and are shown in Figure 12. The frames were chosen by this method in order to optimize coverage and at the same time minimize overlap. Greater picture separation would result in gaps, a lesser separation in more overlap. Mosaicing every third frame gives optimum coverage.

Rectification was accomplished by the method outlined in Appendix A. Essentially, the method is the mathematical solution for the intersection point of a vector with an ellipsoid - the position of the intersection being expressed in latitude and longitude.

GDA63-0046
31 January 1963



Figure 5. Eight Frame Mosaic of TIROS III, Orbit 509



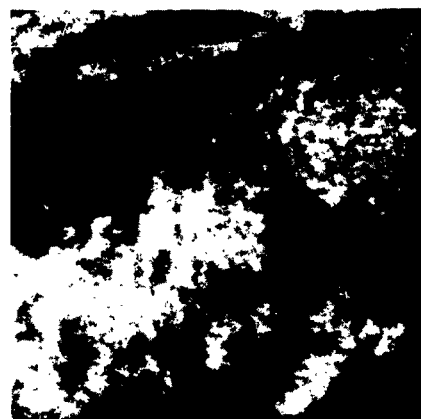
a. Frame 2



b. Frame 5



e. Frame 14



f. Frame 17

2



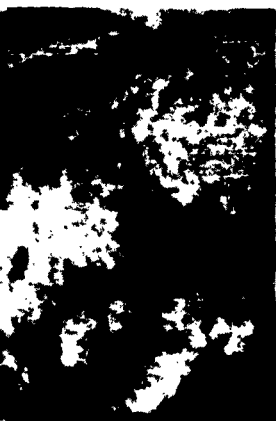
b. Frame 5



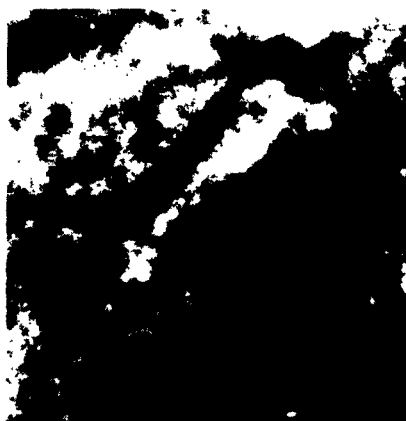
c. Frame 8



d. Frame 11



f. Frame 17



g. Frame 20



h. Frame 23

Figure 6. Digital Display at 120×120 Resolution of Eight Frames of TIROS III, Orbit 509

GDA63-0046
31 January 1963

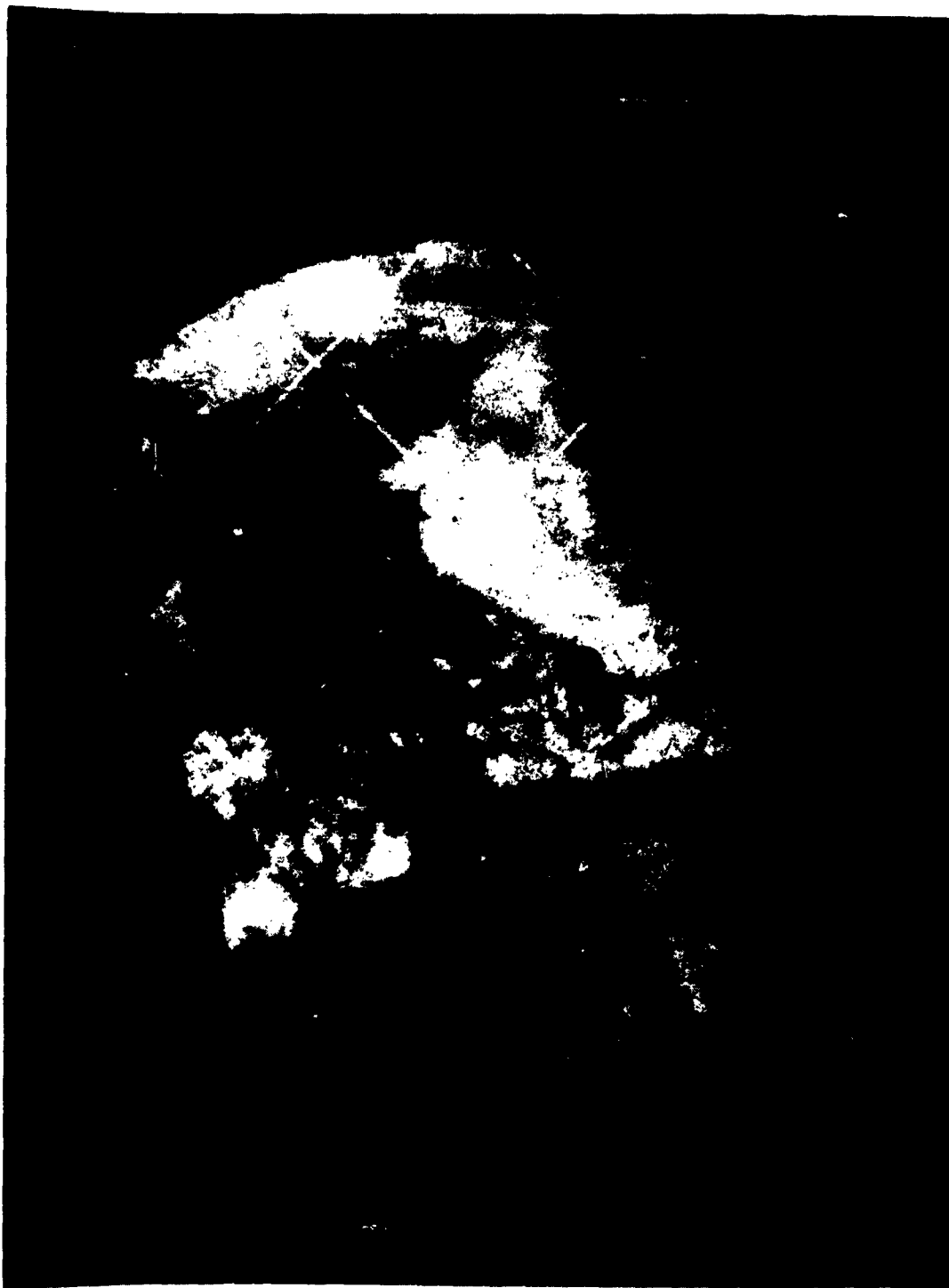
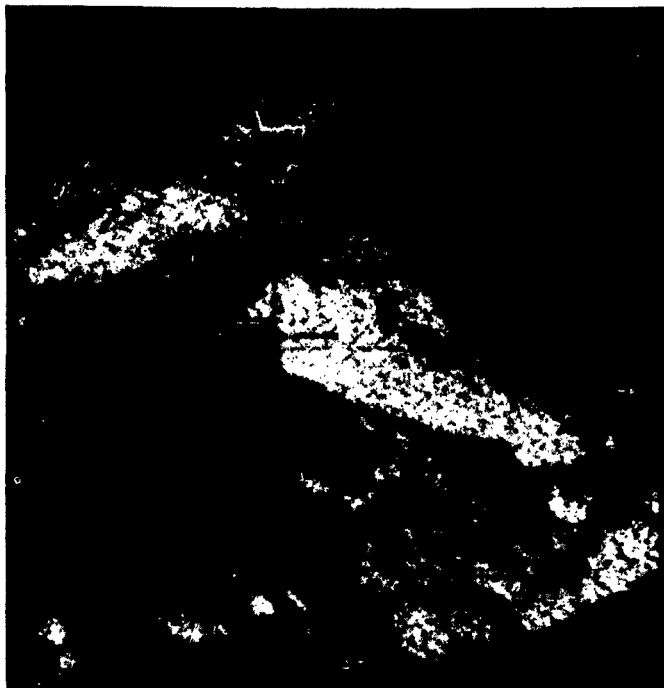
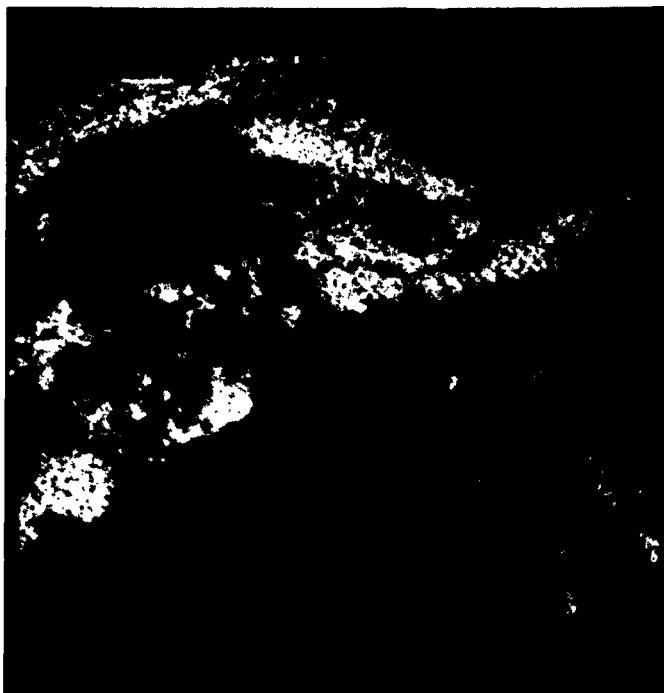


Figure 7. Two Frame Mosaic of TIROS III, Orbit 509



a. Frame 8



b. Frame 11

Figure 8. Digital Display at 240×240 Resolution of Two Frames of TIROS III, Orbit 509

Each picture point is transformed individually to the mapping coordinate space and stored in the computer. Due to the overlap between frames, a point from one frame may be transformed to the same mapping coordinates of a point from another frame. A program option allows either the averaging of two intensity values or the acceptance of one or the other intensity value for points transformed to the same mapping coordinates from two frames. In the rectified mosaics shown in Figure 5 and Figure 7, the first stored intensity value for overlapping frames are accepted.

It should be noted here that filler points were used to fill in the empty spaces caused by rectification. Fill-in is desirable for photointerpretive use of the mosaic display. However, for further computer processing, fill-in would not be required, because missing data points can be accounted for by other methods. Points with an earth incident angle less than 27.5 degrees were not rectified. This corresponds to a maximum nadir angle for TIROS III of 52 degrees and a stretch ratio between points of about three to one. This means that points exhibiting a greater rate of change of earth interior angle with respect to change in nadir angle ($d\omega/d\eta = 0.364$) will not be processed.

Assuming a cloud detail at a height of ten miles to be visible at a 52 degree nadir angle, then rectification will mislocate the data by a distance of about 20 miles. To avoid this, object height could be computed by stereo techniques from pictorial information in the overlap region of two or more frames. Neighborhood correlation could identify a particular detail in both pictures and at the same time determine the stereo shift due to object height.

Due to the storage limitation of the IBM 7090 computer, buffering had to be employed during mosaicing. This was done in the following manner. Two picture frames are rectified and transformed to the mapping coordinate space and stored in the rectilinear memory array. For the 120 line pictures the array consisted of 150×840 mapping points. For the higher resolution 240 line pictures a 300×420 array dimension was used. The first part of the mapping space, where no more overlapping picture points are expected, is rescanned and tape stored for display. The next frame will then be transformed and stored in the array. In this manner the computer memory array advances along the mapping coordinate space. A further buffering problem arises from the finite point array available from the General Dynamics 4020 display device for very long mosaics. The display frame has a 1024×1024 dimension. For an eight frame mosaic of 240×240 resolution pictures, the mapping coordinate space will have to have an array dimension of 300×1260 points, requiring two 4020 frames.

4.3 OUTPUT MAPPING AND GRIDDING, The cloud cover information is displayed in map form, by applying the proper transformation to the latitude and longitude of each rectified point. At present there are five choices of projection which are available.

- a. Polar stereographic.
- b. Oblique stereographic.
- c. Mercator.
- d. Oblique Mercator.
- e. Oblique cylindrical equal-area.

Examples of these are shown in Figures 9, 10, 11, 12, and 13 for the TIROS III, Orbit 509 frame outlines. Each of these projections has its own advantages and peculiarities. The polar stereographic and oblique stereographic projections are useful for displaying rectangular or circular areas near the pole of the projection. These projections are conformal, but the scale changes markedly with distance from the pole of the projection. The oblique mercator differs from the mercator in that the equator of the projection is not the equator of the earth but is an arbitrarily chosen great circle. Mercator projections are conformal, and the scale changes with the distance from the equator of the projection. Mercator projections are useful for the display of information that is concentrated along a great circle; for then the equator of the projection can be chosen as that great circle; and change in scale over the mapped area is small. The oblique cylindrical equal area projection is similar to the oblique mercator except that it has the property that equal areas on the map correspond to equal areas on the earth. The projection is non-conformal, with the distortion of shapes and change in scale increasing with distance from the equator of the projection.

Another subroutine creates grid lines in latitude and longitude spaced five degrees apart, over the display area, which may be of any size, of any rectangular shape, centered at any desired latitude and longitude. Additional subroutines are planned which will add other mapping projections to the above list. Continental coastlines can be displayed on all map projections. Figure 14 shows two displays of perspective views of the earth and the track of TIROS III, Orbit 509 and 510, with continental outlines generated by the computer from stored outline data.

TIROS III. FRAMES 23, 20, 17, 14, 11, 8, 5, AND 2 OF ORBIT 509. POLAR STEREOGRAPHIC PROJECTION.

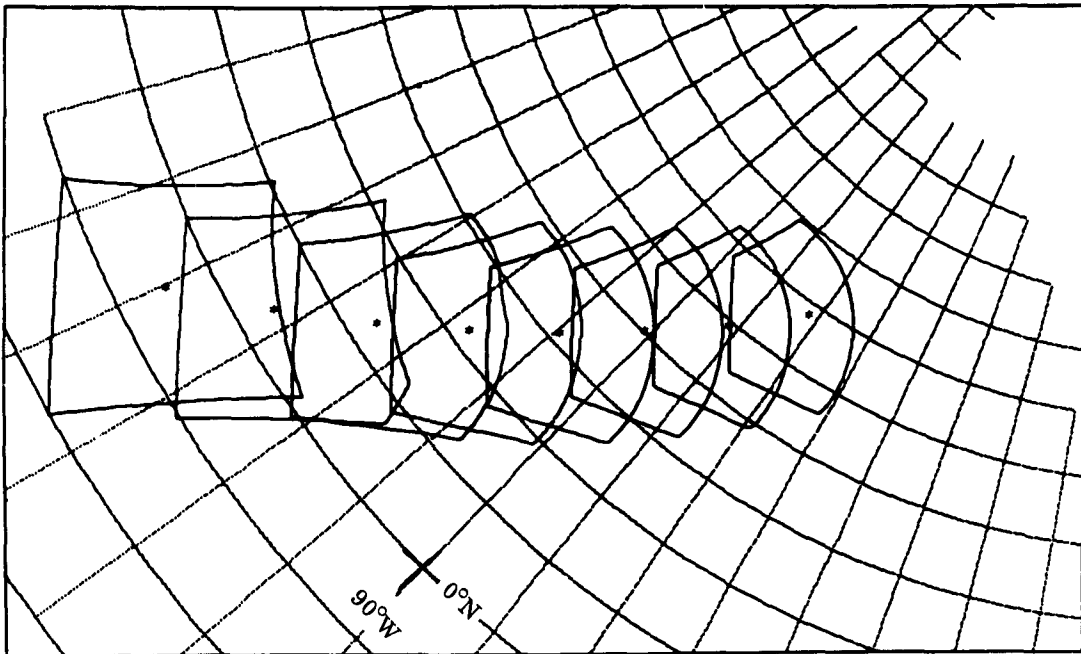


Figure 9. Polar Stereographic Map

TIROS III. FRAMES 23, 20, 17, 14, 11, 8, 5, AND 2 OF ORBIT 509. OBLIQUE STEREOGRAPHIC PROJECTION.

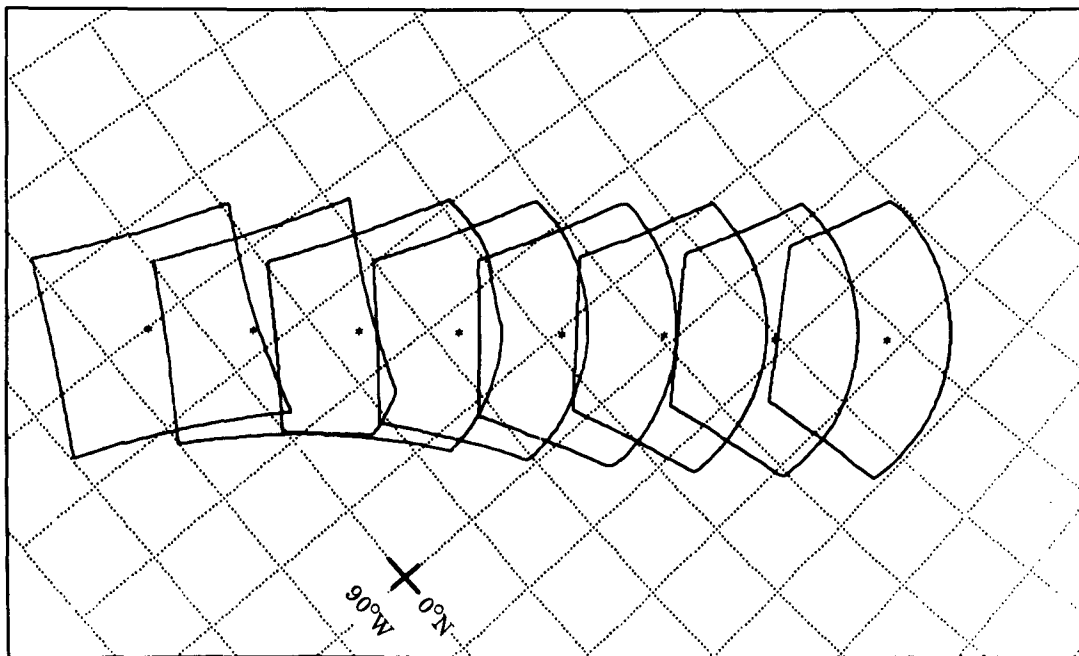


Figure 10. Oblique Stereographic Map

TIRDS III. FRAMES 23, 20, 17, 14, 11, 8, 5, AND 2 OF ORBIT 509. MERCATOR PROJECTION.

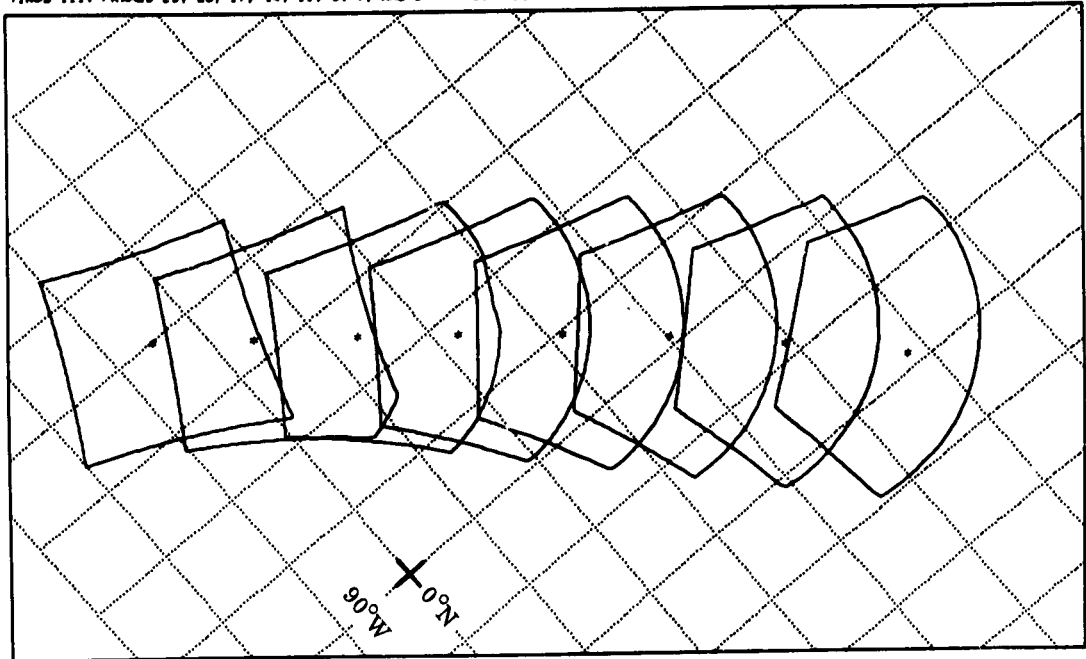


Figure 11. Mercator Map

TIRDS III. FRAMES 23, 20, 17, 14, 11, 8, 5, AND 2 OF ORBIT 509. OBLIQUE MERCATOR PROJECTION.

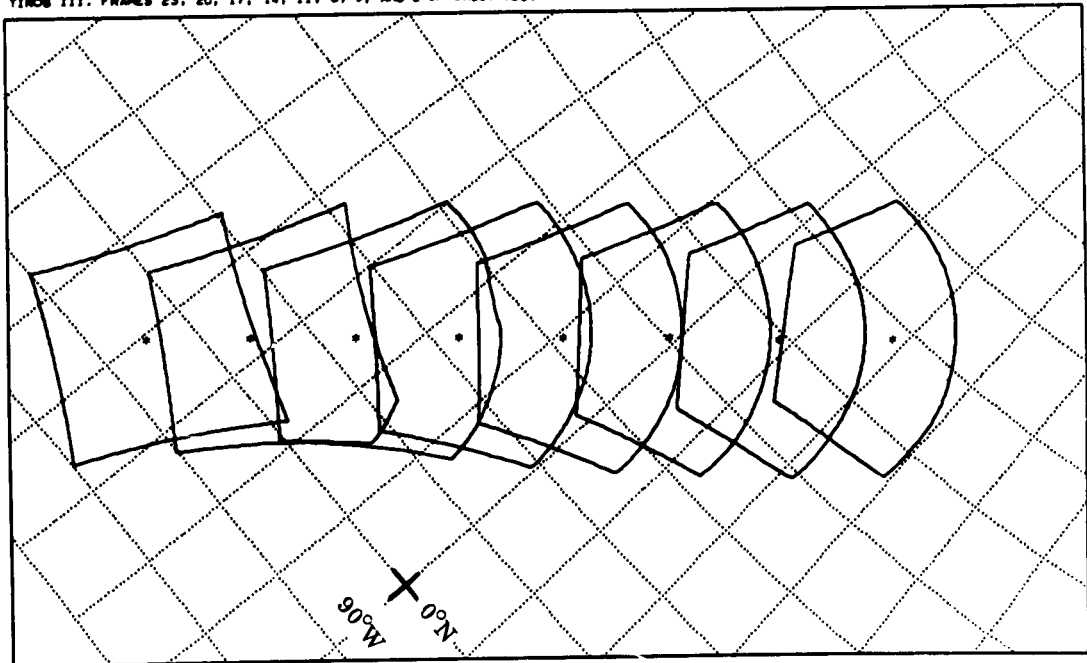


Figure 12. Oblique Mercator Map

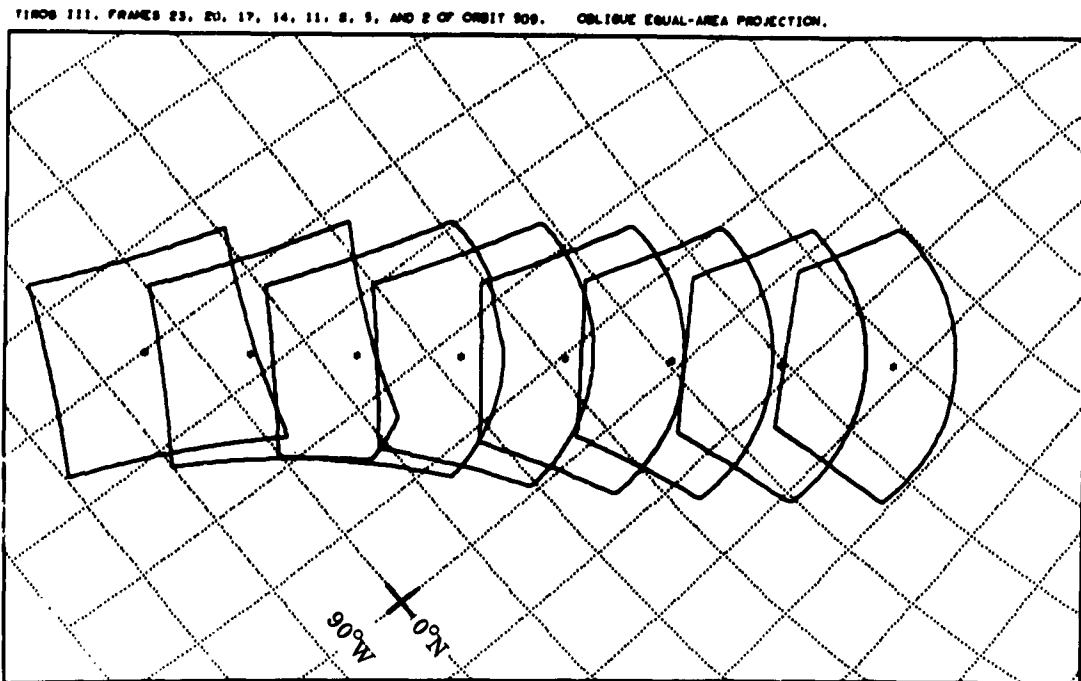


Figure 13. Oblique Cylindrical Map With Equal Area Scaling

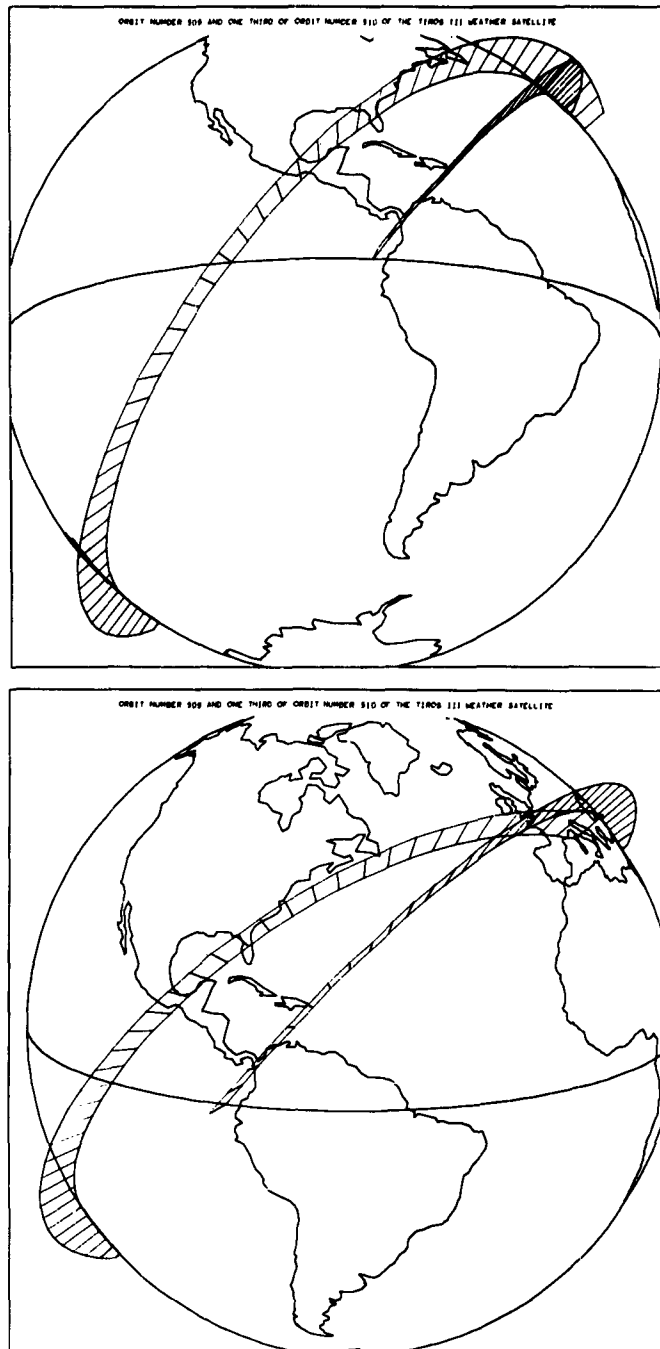


Figure 14. Oblique Views of Earth and TIROS III, Orbit 509 and 510 Track

SECTION 5 DATA ANALYSIS

The question as to what data analyses can be performed on meteorological satellite data was investigated and some approaches to simple pictorial analysis techniques were attempted.

The pictorial analysis of digitized intensity data as obtained from the TIROS TV camera system is termed intensity manipulation. The analysis of several electromagnetic sensor channel data, channels such as the visual and infrared radiation channels, is defined as multiple spectral correlation. In this section, various intensity manipulation techniques are described. A most promising and meteorologically useful processing output, an automatic nephanalysis, is discussed.

5.1 INTENSITY MANIPULATIONS

5.1.1 Intensity Normalization. It is anticipated that intensity normalization will be required in analytical processes designed to operate on pictorial intensity values. Intensity normalization is the process applied to pictorial data to correct for intensity variations due to the light transmission and sensing systems, thereby obtaining higher accuracy object intensity values. Furthermore, in a meteorological satellite cloud picture, intensities acquired from detail at greater slant range can be expected to decrease. The corrections for this limb darkening effect and for intensity variations due to solar illumination distribution have not as yet been included in the pictorial processing but are recognized as a necessity for meaningful intensity manipulations in an operational processing system.

5.1.2 Pictorial Intensity Differentiation. The determination and usefulness of intensity boundary points in a picture has been evaluated. A boundary point is defined as a picture point within a neighborhood with non-zero intensity differential. This process differentiates the intensities over the picture, thereby, enhancing the changes within the picture for photointerpretive uses and possibly reducing the number of bits required for transmission or for storing the picture in a computer.

The differential method is illustrated in Figure 15. The picture point with intensity value I_0 , is called an intensity boundary point if $I_E - I_W \neq 0$ or $I_N - I_S \neq 0$. In the process the intensities of all boundary points are retained and can be displayed pictorially with or without intensity modulation. Figure 16a shows the original picture, TIROS I, Orbit 16, Frame 24. Figure 16b is the display without intensity modulation of approximately half of the resultant intensity boundary points. In Figure 16c all resultant boundary points are displayed with intensity modulation. It can be stated that the degree to which pictorial enhancement is achieved from pictorial differentiation

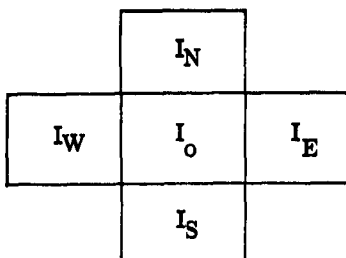


Figure 15. Boundary Point Neighborhood

is small or non-existent especially in light of the greater resultant noise enhancement. The process tends to emphasize small variations, which for noisy pictures can be detrimental to quality. It should be noted here, that the intensity values did not undergo any normalization corrections.

5.1.3 Intensity Contouring. Picture differentiation by means of boundary point determination loses essential pictorial data by ignoring the direction of the intensity differential, and, thereby, makes it impossible to correctly connect adjacent boundary points into equal intensity contours. To avoid this problem, intensity contouring was investigated by a method which retains both the magnitude and direction of the intensity differential.

A vectoring technique was employed to create intensity contours. The picture when stored in the computer is analyzed by determining for all 2×2 neighborhoods in the picture the direction vectors of any existing intensity contours. For each elemental contour vector, the position, direction, intensity and the gradient magnitude are determined by the contouring program. A contour vector in a 2×2 array of points is defined as a line connecting two points of equal effective intensity keeping a point of lower intensity to the left of the vector. This assures that the intensity gradient is normal to the vector direction. The origin of an intensity vector is coincident with the terminus of the previous vector. In this manner an intensity contour consists of a string of equal intensity vectors describing the outer equal intensity bounds of a picture area in a sequential clockwise rotational manner. Results of this process can be likened to the height contours of topographical maps.

Figure 17 illustrates the basic vectoring technique. The vector coding is defined by Figure 17a. Figure 17b represents two examples of 2×2 neighborhoods of four intensity values, which in Figure 17c are rank ordered and in Figure 17d are rotated in a counter-clockwise direction until, for each example, the first lowest intensity encountered is located in a reference field. The resulting sequences of four numbers are normalized and rotated representations of the neighborhoods which serve as characteristic search words in a search table. By this technique of normalization and limited rotation only 26 cases or combinations of values remain. For the finite

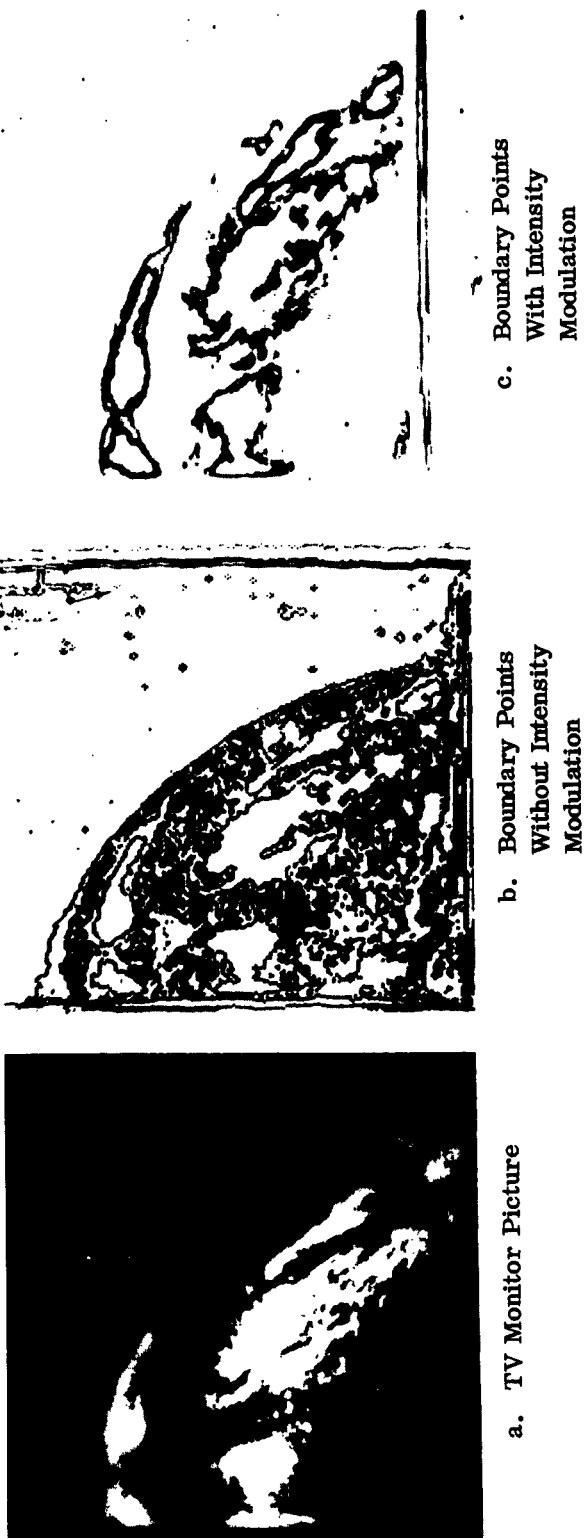


Figure 16. TV Monitor Picture of TIROS I, Orbit 16, Frame 24 and Boundary Points Displayed With and Without Intensity Modulation

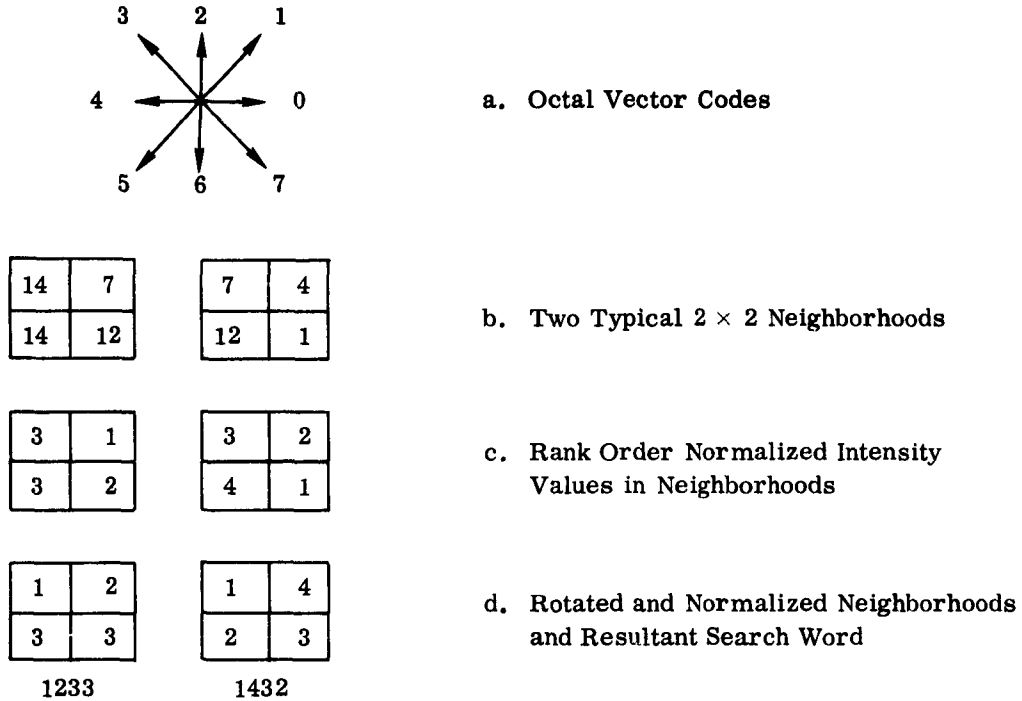


Figure 17. Determining Intensity Contour Segments From 2×2 Picture Neighborhoods

number of cases only seven types of vectors exist, which are illustrated in Figure 18. The search table shown in Table 2 gives the normalized vector directions, intensities, and gradient values of all intensity contour vectors possible in the 2×2 neighborhoods. These are subsequently converted back to the exact values of intensity, vector direction and vector origin by a clockwise rotation equal to that incurred during normalization and rotation.

An example of pictorial intensity contouring is included. Figure 19a is the input picture (taken on NASA unmanned Mercury spacecraft, MA4) showing a portion of the West African coast. This picture was scanned and digitized to 120×120 picture elements each with 16 intensity levels and subsequently contoured by the technique described above. A separate contour is determined and displayed for each intensity level in Figure 19b. Overlapping intensity contours increases the effective displayed brightness in regions with high intensity gradient. The computer process determined 1906 intensity contours with an average length of about 8 vectors. Each contour has associated with it a starting position within the display area, which for a 120×120 picture requires 14 bits per contour or 26,684 bits for the example. Each vector requires 3 bits to assign to it one of the eight possible directions, which for the case under discussion results in 45,704 bits. Therefore, 72,388 bits are required to describe the contoured picture. The original digitized picture has 4 bits per point resulting in 57,600

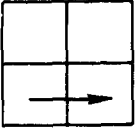
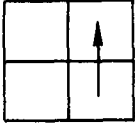
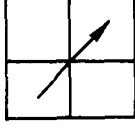
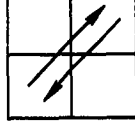
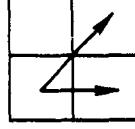
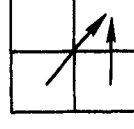
NORMALIZED 2 × 2 NEIGHBORHOOD	SEARCH WORD	VECTOR	TYPE VECTOR				
<table border="1"><tr><td>1</td><td>1</td></tr><tr><td>1</td><td>1</td></tr></table>	1	1	1	1	1111		No Vector
1	1						
1	1						
<table border="1"><tr><td>1</td><td>1</td></tr><tr><td>2</td><td>2</td></tr></table>	1	1	2	2	1122		0 Type
1	1						
2	2						
<table border="1"><tr><td>1</td><td>2</td></tr><tr><td>1</td><td>2</td></tr></table>	1	2	1	2	1221		2 Type
1	2						
1	2						
<table border="1"><tr><td>1</td><td>2</td></tr><tr><td>2</td><td>2</td></tr></table>	1	2	2	2	1222		1 Type
1	2						
2	2						
<table border="1"><tr><td>1</td><td>2</td></tr><tr><td>2</td><td>1</td></tr></table>	1	2	2	1	1212		1 and 5 Type
1	2						
2	1						
<table border="1"><tr><td>1</td><td>2</td></tr><tr><td>3</td><td>3</td></tr></table>	1	2	3	3	1233		1 and 0 Type
1	2						
3	3						
<table border="1"><tr><td>1</td><td>3</td></tr><tr><td>2</td><td>3</td></tr></table>	1	3	2	3	1332		1 and 2 Type
1	3						
2	3						

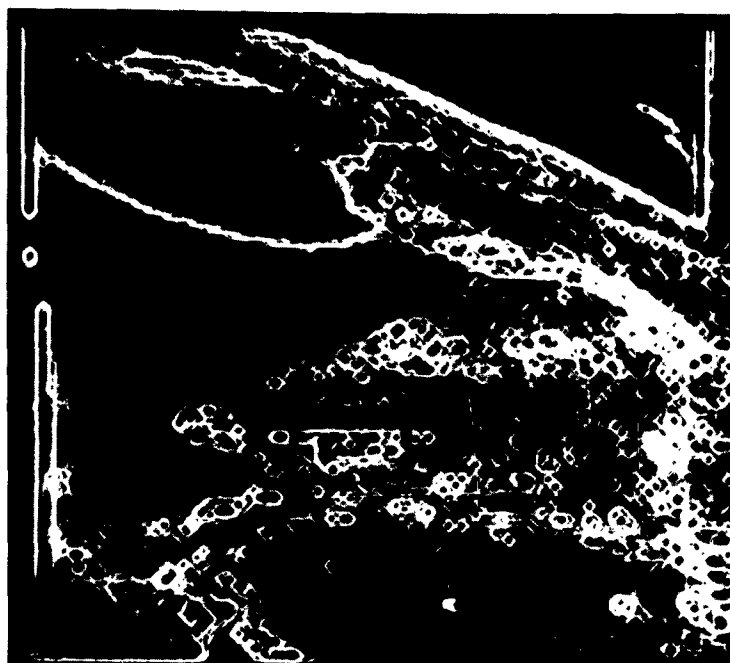
Figure 18. Vector Types Possible in 2 × 2 Neighborhoods

Table 2. Vector Characteristic Search Table

SEARCH WORD	VECTOR 1			VECTOR 2		
	TYPE	I RANK	GRADIENT Δ I RANK	TYPE	I RANK	GRADIENT Δ I RANK
1111	NONE					
1112	NONE					
1121	NONE					
1211	NONE					
1122	0	2	2-1			
1221	2	2	2-1			
1212	1	2	2-1	5	2	2-1
1123	0	2	2-1			
1132	0	2	2-1			
1231	2	2	2-1			
1321	2	2	2-1			
1213	1	2	2-1	5	2	2-1
1312	1	2	2-1	5	2	2-1
1222	1	2	2-1			
1233	1	2	2-1	0	3	3-2
1323	1	3	3-1	5	3	3-2
1332	1	2	2-1	2	3	3-2
1223	1	2	2-1			
1232	1	2	2-1			
1322	1	2	2-1			
1234	1	2	2-1	0	3	3-2
1243	1	2	2-1	0	3	3-2
1423	1	3	3-1	5	3	3-2
1432	1	2	2-1	2	3	3-2
1342	1	2	2-1	2	3	3-2
1324	1	3	3-1	5	3	3-2



a. Photograph



b. Intensity Contours

Figure 19. Photograph and Intensity Contours of West African Coast
Taken From Unmanned Mercury Spacecraft, MA4

bits. It can be concluded that for large amounts of detail in a meteorological satellite picture a multiplicity of contours exist. This appears to limit the usefulness of this contouring technique to certain applications in which pictorial data was previously processed and fewer levels were retained.

5.1.4 Intensity Contour Filter. An attempt was made to separate cloud from background by means of contour filtering. This is dependent upon coincidence of cloud edges and high gradients. The gradient magnitudes of the vectors making up the contours can be statistically evaluated, and a decision as to whether a contour is to be retained or rejected can be made by means of a threshold value and the averaged gradient of all vectors in a contour. In the vicinity of a cloud edge, however, there are a large number of contours, each with a relative low average gradient and not uniquely distinguishable. This technique may have merit for single contours exhibiting high gradients. Other investigations indicate that characterizations of certain cloud outline shapes are possible by the vectored outline method, this may eventually result in the recognition of streamlines or vortices.

5.1.5 Intensity - Height Determination. It is difficult, if not impossible, to imply height information at this time from pictorial intensity contours. A photointerpreter can on occasion see a degree of vertical structure by shadowing. The possibility exists that cloud height determination is possible by means of stereo and neighborhood intensity auto-correlation techniques. Further work is required to prove this possibility.

5.1.6 Cloud Separation by Intensity Slicing. Cloud separation by means of intensity slicing can at best be an approximate method. It was employed for the cloud amount determination reported in the next section. However, assuming intensity normalized data, and setting a constant intensity threshold, very dim clouds would be entirely missed with a medium threshold. With a low threshold it is likely that more land areas are included in addition to clouds. In desert regions, in ice and snow covered regions, and in areas with sun-water reflections, in cases where the local visual albedo is high, a threshold for intensity slicing and consequent cloud separation becomes meaningless.

5.2 CLOUD AMOUNT DETERMINATION. The method used to determine the cloud amount per unit area is basically an area integration technique, in which the pictorial data in the rectified-mosaic map projection is partitioned into a rectilinear array of elemental areas. Each of these elemental areas, which may contain any number of data points, represents an equal area on the surface of the earth if an equal area cylindrical projection is used as the mapping plane. Due to the stretching of data caused by rectification, there will be points in the mapping plane without any data. If such points are defined as null points (N), they can then be properly accounted for during integration. The intensity values of data points are sliced in order to get a simulated cloud/no-cloud decision. If M is the maximum number of points in the array, C is one

cloud element and N is a no-data point or null point, then the cloud amount of one elemental area is given by:

$$\text{Percent cloud amount} = (\Sigma C)/(M - \Sigma N)$$

Another value estimated is the percent data amount:

$$\text{Percent data amount} = (M - \Sigma N)/M$$

This value is retained for each elemental area along with percent cloud amount and gives an estimate of the reliability of the percent cloud amount. The percent cloud amount is determined for each elemental area in the presence of null points and has the nature of a best estimate for the given data. This means that to the part of the elemental area with null points, the same cloud/no-cloud distribution as determined from among the data points can be assigned. In this manner, no fill-in of null points is required. For elemental areas with a smaller percent data amount than a specified threshold, the reliability of the best estimate is deemed too low. The elemental area is then eliminated from the analysis.

Figure 20 shows the printed result of the above described process when applied to the rectified mosaic of TIROS III, Orbit 509. The oblique cylindrical equal area map was partitioned into 6×6 elemental areas, which represents an approximately 1000 square mile area. Intensity slicing was chosen arbitrarily at an intensity level of 7 out of 15 levels, and the cloud amount data of an elemental area was retained only, if more than 30 percent data amount is available. The percent cloud amount was rounded to numbers between 0 and 10 to give cloud amount in tenths. Equal cloud amount contours were determined by the intensity contouring program and subsequently displayed on the General Dynamics 4020, as shown in Figure 20c. The only cloud amount contours displayed are those for areas with 20, 50 and 80 percent cloud amount. Different display intensities were used for the three sets of contours, in order to enable distinguishing between them. The nephanalysis for TIROS III, Orbit 509/508 is included in Figure 21. Although the location of the neph appears to be approximately 8 degrees longitude further east than the rectified mosaic, shown in Figure 7 and again in Figure 20a, it allows the comparison with and evaluation of the cloud amount contouring process.

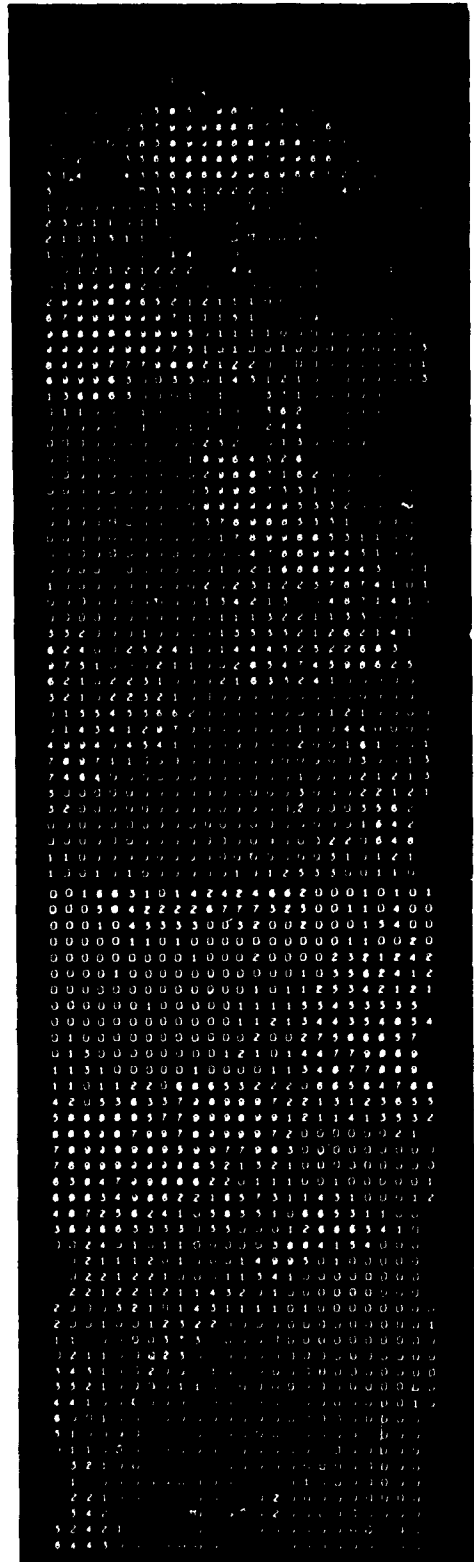
Some further processes can be performed on each elemental area by considering the spatial cloud distribution within the elemental area. The method proposed is based on a limited amount of contouring within each elemental area to determine the number of cloud contours. For instance, if all the cloud data within an elemental area was grouped so that only one contour was determined, then the cloud distribution approximates an overcast condition - unless the cloud amount was too small. Two parameters for the decision process could be used: percent cloud amount and the number of contours. It should be pointed out again that the investigations of these analysis techniques assume the positive identification or simulation of cloud areas.

31 January 1963

5.3 SPECTRAL CORRELATION. Studies into the possibilities of visual and infrared spectral correlation techniques for the identification of cloud have been initiated. Other possibilities for the processing of the TIROS infrared data are aimed at aiding research presently conducted by manual and semi-automatic methods. The requirements for a generalized spectral correlation process are being formulated. Future reports will discuss results of this study phase.

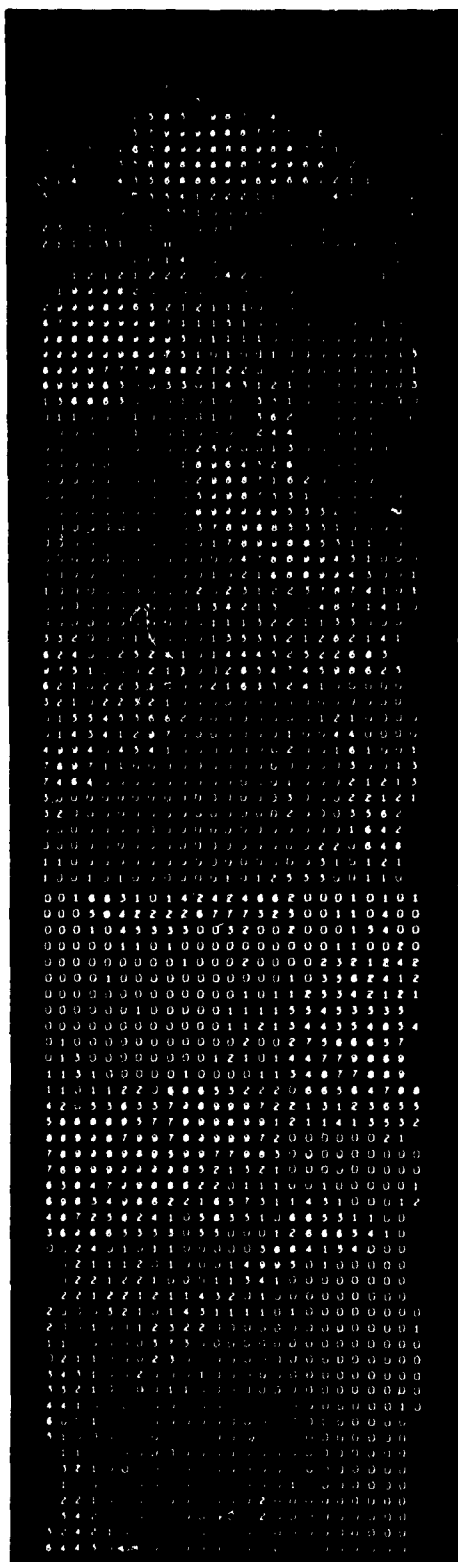


a. Rectified - Eight Frame Mosaic

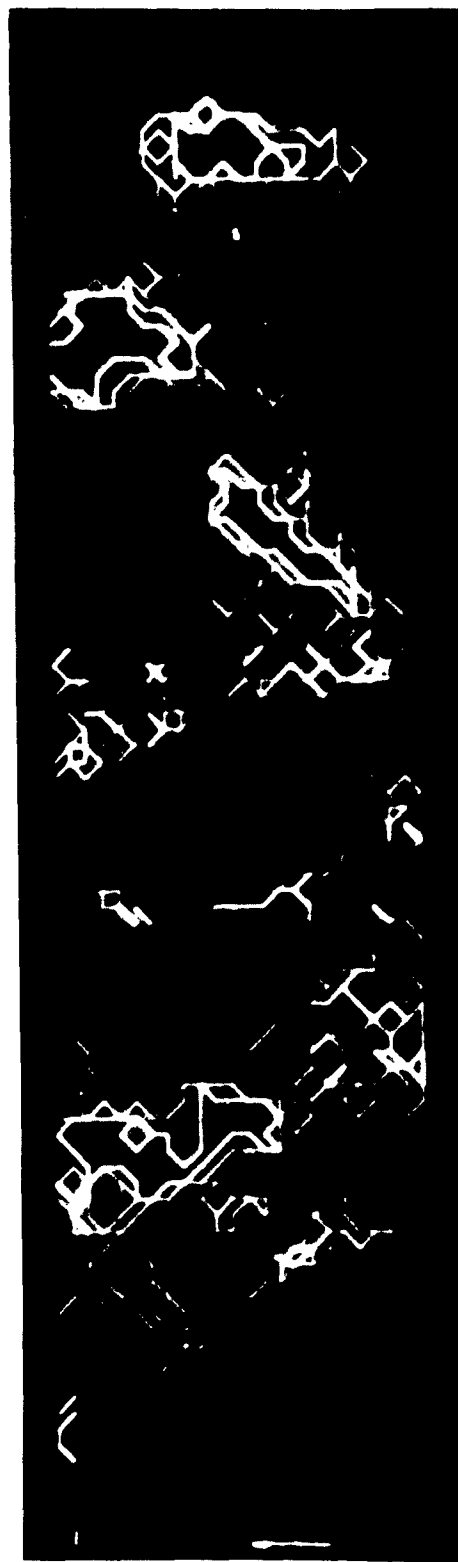


b. Cloud Amount in Tenths for 1000 Square Mile Areas

Figure 20. Cloud Cover Analysis for Eight Frame Mosaic of TIROS III, Orbit



b. Cloud Amount in Tenths for
1000 Square Mile Areas



c. 20, 50 and 80 Percent Cloud
Amount Contours

SECTION 6
INFORMATION PRESENTATION

The operational direct use of the meteorological satellite pictorial data is of course limited to a number of highly experienced analysts, who none the less have to perform a great number of routine tasks connected with the utilization of such data. It is almost certain that reliably rectified-mosaiced TV data displayed on a useful map projection would be highly welcome by meteorological analysts. It is also believed that there is a need for low resolution hemispheric and possibly global cloud coverage maps generated by means of the described rectification-mosaic process. Highest resolution may be required by an analyst only for certain limited regions. He may then be interested in much smaller geographical coverage, so that single high resolution rectified and displayed frames could fill his need.

One of the best promises of automatic meteorological satellite data processing is in data analysis and information presentation. The method for presenting the extracted information from nephanalyses, or cloud top temperature and hence height analyses should transmit to the analyst or user the maximum amount of information in the most efficient manner. Meteorologists have long used contours on conventional weather maps for presenting information efficiently. These contours or isolines are readily assimilated by the user and have herein a tremendous advantage over numerically listed and tabulated information. The previously described contouring process enables the automatic presentation of contoured information. The contoured cloud amount mosaic, shown in Figure 20c, represents the first solid step in this direction.

SECTION 7
CONCLUSION

It should be pointed out in closing that the techniques described here are equally applicable to data obtained from any scan-type satellite sensor, be it optical, video, infrared, etc. Also, simulation and verification of these processes will aid in determining their usefulness, which must partially define the requirements of future automatic meteorological data processing systems.

However, much work still needs to be done, primarily to further define the processes which are pertinent to cloud distribution and cloud type classifications. These include texture analysis, cloud and weather system motion, and the vast and still largely unknown field of infrared data analysis and correlation.

SECTION 8
REFERENCES

1. Documentation for TIROS III Television Data; U.S. Department of Commerce, Weather Bureau Meteorological Satellite Laboratory Report 9, Washington, D. C.; 1962
2. Goldshlak, Leon; TIROS III Attitude Summary; Allied Research Associates; Boston, Massachusetts; 1962
3. GRD Research Notes Number 36; Edited by William K. Widger, Jr.; Contributions to Satellite Meteorology; 1960.
4. TIROS I Meteorological Satellite System, Final Comprehensive Technical Report; RCA; Princeton, New Jersey; 1961.
5. Glaser, Arnold H.; TIROS I: An Operational Evaluation of a new Meteorological Tool; Allied Research Associates, Inc; Boston Massachusetts; 1960.
6. Wexler, Raymond; Interpretation of TIROS II Radiation Measurements; Allied Research Associates; Inc; Boston, Massachusetts; 1962.
7. Conover, John H.; Cloud Interpretation from Satellite Altitudes; CRL Research Note Number 81; 1962.

APPENDIX A
RECTIFICATION MATHEMATICS

If we assume an ellipsoidal earth, any point on the earth can be given by the coordinates X, Y, and Z where these coordinates satisfy the equations

$$X = a \cos \theta \cos \lambda$$

$$Y = a \cos \theta \sin \lambda$$

and

$$Z = b \sin \theta$$

In these equations, a and b are the equatorial and polar radii, respectively, λ is the longitude (measured positive west), and θ is the parametric variable of the meridional ellipse.

A point on the surface of the earth will have coordinates in two systems: the earth system and the camera system. The earth system is defined as an earth-centered right-handed system with the x axis passing through the Greenwich meridian and the z axis passing through the north pole. The camera system is defined as a right-handed system with the x-y plane parallel to the camera plate, and the z axis pointing toward the earth and coincident with the optical axis of the camera (see Figure A-1).

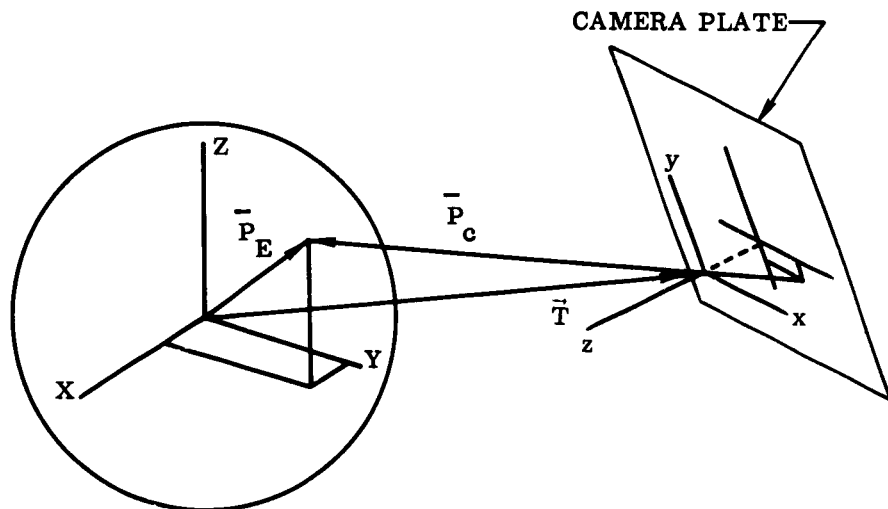


Figure A-1. The Earth System and the Camera System

We will consider an individual point on the camera plate. This point has coordinates $x, y, -1$, where x and y are expressed in units of one focal length of the equivalent pinhole camera.

The direction cosines of the vector from the camera to the corresponding point on the ground in the camera system are

$$l = \frac{-x}{\sqrt{x^2 + y^2 + 1}}$$

$$m = \frac{-y}{\sqrt{x^2 + y^2 + 1}}$$

and

$$n = \frac{1}{\sqrt{x^2 + y^2 + 1}}$$

The vector position of the point on the earth in the camera system will be

$$\vec{P}_c = d(l\vec{i} + m\vec{j} + n\vec{k})$$

where d is the unknown distance from the camera to the point. Rotating the vector to the earth system, and adding the vector representing the camera position in the earth system gives us the position vector of the point in the earth system:

$$\begin{bmatrix} \vec{P}_E \end{bmatrix} = \begin{bmatrix} M \end{bmatrix} \begin{bmatrix} \vec{P}_c \end{bmatrix} + \begin{bmatrix} \vec{T} \end{bmatrix}$$

The rotation matrix M and the translation vector T are given. We have

$$\vec{P}_E = (dl + p)\vec{i} + (dm + q)\vec{j} + (dn + r)\vec{k}$$

In the last equation, $p, q,$ and r are the components of T ; and $l, m,$ and n are now the direction cosines of the vector from the camera to the earth point in the earth system. We now have the relationships

$$dl + p = a \cos \theta \cos \lambda$$

$$dm + q = -a \cos \theta \cos \lambda$$

and

$$dn + r = b \sin \theta$$

Squaring both sides of the above equation and adding, we have

$$d^2(\ell^2 + m^2 + n^2) + p^2 + q^2 + r^2 + 2d(\ell p + m q + n r) = a^2 \cos^2 \theta + b^2 \sin^2 \theta$$

So

$$d^2(\ell^2 + m^2 + n^2) + 2d(\ell p + m q + n r) - a^2 + (n^2 - b^2) \sin^2 \theta + q^2 + q^2 + r^2 = 0$$

Using the relationship $dn + r = b \sin \theta$, we have

$$d^2(\ell^2 + m^2 + n^2) + 2d(\ell p + m q + n r) - a^2 + \frac{a^2 - b^2}{b^2} (dn + r)^2 + p^2 + q^2 + r^2 = 0$$

or

$$d^2(\ell^2 + n^2 + \frac{a^2}{b^2} n^2) + 2d(\ell p + m q + \frac{a^2}{b^2} n r) + p^2 + q^2 + \frac{a^2}{b^2} r^2 - a^2 = 0$$

If we let

$$\vec{V} = \ell \vec{i} + m \vec{j} + \frac{a}{b} n \vec{k}$$

and

$$\vec{S} = p \vec{i} + q \vec{j} + \frac{a}{b} r \vec{k}$$

then our equation becomes

$$(\vec{V} \cdot \vec{V}) d^2 + 2d(\vec{V} \cdot \vec{S}) + (\vec{S} \cdot \vec{S}) - a^2 = 0$$

The solution for d is

$$d = \frac{-(\vec{V} \cdot \vec{S}) - \sqrt{(\vec{V} \cdot \vec{S})^2 - (\vec{V} \cdot \vec{V}) (\vec{S} \cdot \vec{S} - a^2)}}{\vec{V} \cdot \vec{V}}$$

The quantity under the radical is proportional to the sines of the incidence angle. When the incidence angle is smaller than the minimum tolerable angle, rectification for the respective picture point terminates.

Using the value for d we can find X, Y, and Z in the earth coordinate system.

<p>Geophysics Research Directorate, Air Force Cambridge Research Laboratories, Office of Aerospace Research, Bedford, Massachusetts Rpt No. AFCRL-TDR-63-243. AUTOMATIC DATA PROCESSING OF WEATHER SATELLITE DATA, by W. A. Marggraf, 31 January 1963, 49 pp incl illus and photographs.</p> <p>Unclassified report</p> <p>The computer processes studied include ingestion of satellite pictorial data with digitization and digital pictorial display; data location, which includes rectification, automatic mosaicing, and mapping transformations;</p> <p style="text-align: center;">○</p>	<p>UNCLASSIFIED</p> <p>1. Meteorological data 2. Data processing systems 3. Satellites I. AFCRL Project 6698 II. Contract AF 19(604)-8861 III. General Dynamics/Astronautics, San Diego, Calif. IV. W. A. Marggraf V. Avl fr OTS VI. In ASTIA collection</p>	<p>UNCLASSIFIED</p> <p>1. Meteorological data 2. Data processing systems 3. Satellites I. AFCRL Project 6698 II. Contract AF 19(604)-8861 III. General Dynamics/Astronautics, San Diego, Calif. IV. W. A. Marggraf V. Avl fr OTS VI. In ASTIA collection</p>	<p>UNCLASSIFIED</p> <p>1. Meteorological data 2. Data processing systems 3. Satellites I. AFCRL Project 6698 II. Contract AF 19(604)-8861 III. General Dynamics/Astronautics, San Diego, Calif. IV. W. A. Marggraf V. Avl fr OTS VI. In ASTIA collection</p>
<p>and data analysis, such as differentiation, slicing, and contouring of the data from pictorial intensity, and cloud amount determination. Data from TIROS III, Orbit 509 frames is used to demonstrate the techniques and results of rectification, mosaicing, and cloud cover amount determination. Also included are examples of reduced and full resolution digitized TIROS TV pictures.</p> <p style="text-align: center;">○</p>	<p>UNCLASSIFIED</p> <p>and data analysis, such as differentiation, slicing, and contouring of the data from pictorial intensity, and cloud amount determination. Data from TIROS III, Orbit 509 frames is used to demonstrate the techniques and results of rectification, mosaicing, and cloud cover amount determination. Also included are examples of reduced and full resolution digitized TIROS TV pictures.</p>	<p>UNCLASSIFIED</p> <p>and data analysis, such as differentiation, slicing, and contouring of the data from pictorial intensity, and cloud amount determination. Data from TIROS III, Orbit 509 frames is used to demonstrate the techniques and results of rectification, mosaicing, and cloud cover amount determination. Also included are examples of reduced and full resolution digitized TIROS TV pictures.</p>	<p>UNCLASSIFIED</p> <p>and data analysis, such as differentiation, slicing, and contouring of the data from pictorial intensity, and cloud amount determination. Data from TIROS III, Orbit 509 frames is used to demonstrate the techniques and results of rectification, mosaicing, and cloud cover amount determination. Also included are examples of reduced and full resolution digitized TIROS TV pictures.</p>